

Article

Role of Mg Impurity in the Water Adsorption over Low-Index Surfaces of Calcium Silicates: A DFT-D Study

Chongchong Qi ^{1,2,3}, Qiusong Chen ^{1,*} and Andy Fourie ²

¹ School of Resources and Safety Engineering, Central South University, Changsha 410083, China; chongchong.qi@research.uwa.edu.au

² School of Civil, Environmental and Mining Engineering, University of Western Australia, Perth 6009, Australia; andy.fourie1@uwa.edu.au

³ School of Molecular Sciences, University of Western Australia, Perth 6009, Australia

* Correspondence: qiusong.chen@csu.edu.cn

Received: 5 June 2020; Accepted: 21 July 2020; Published: 26 July 2020



Abstract: Calcium silicates are the most predominant phases in ordinary Portland cement, inside which magnesium is one of the momentous impurities. In this work, using the first-principles density functional theory (DFT), the impurity formation energy (E_{for}) of Mg substituting Ca was calculated. The adsorption energy (E_{ad}) and configuration of the single water molecule over Mg-doped β -dicalcium silicate (β -C₂S) and M3-tricalcium silicate (M3-C₃S) surfaces were investigated. The obtained Mg-doped results were compared with the pristine results to reveal the impact of Mg doping. The results show that the E_{for} was positive for all but one of the calcium silicates surfaces (ranged from -0.02 eV to 1.58 eV), indicating the Mg substituting for Ca was not energetically favorable. The E_{ad} of a water molecule on Mg-doped β -C₂S surfaces ranged from -0.598 eV to -1.249 eV with the molecular adsorption being the energetically favorable form. In contrast, the E_{ad} on M3-C₃S surfaces ranged from -0.699 eV to -4.008 eV and the more energetically favorable adsorption on M3-C₃S surfaces was dissociative adsorption. The influence of Mg doping was important since it affected the reactivity of surface Ca/Mg sites, the E_{ad} of the single water adsorption, as well as the adsorption configuration compared with the water adsorption on pristine surfaces.

Keywords: calcium silicates; first-principles DFT; Mg doping; water adsorption; structural and electronic properties

1. Introduction

Population growth has driven the exponential increase in infrastructure demand, especially in developing countries like China and India [1,2]. As the main ingredients within construction materials, ordinary Portland cement (OPC) is thus attracting considerable attention. Many studies have been conducted not only for the efficient use of OPC, but also to reduce energy consumption and CO₂ emission during OPC production [3,4]. However, the fine-tuning of OPC requires a more fundamental understanding of its hydration mechanism, which is vital for the sustainable development of the cement industry and effective application of cement-based materials [5].

OPC consists of four main compounds, namely alite (50–70 wt.%), belite (15–30 wt.%), aluminate (5–10 wt.%), and ferrite (5–15 wt.%). Alite and belite are the impurity-modified constituents of tricalcium silicate (Ca₃SiO₅ or C₃S) and dicalcium silicate (Ca₂SiO₄ or C₂S), respectively. In contrast to aluminate (Ca₃Al₂O₆) and ferrite (Ca₂Al_xFe_{2-x}O₅, $0 \leq x \leq 1.4$) [6], C₃S and C₂S are often referred to as calcium silicates and, in most cases, control the hydration characteristics of OPC [7]. Since phenomenological

experiments could only provide an overall indicator for the cement hydration reactions, the theoretical method is a promising alternative to reveal the hydration mechanism of calcium silicates [8].

The structural and electronic properties of calcium silicates have been theoretically investigated using first-principles calculations or molecular dynamics [9–15]. For example, Durgun et al. [16] utilized first-principles calculations to reveal the relationship between the reactivity and electronic structure of calcium silicates. It was found that the high reactivity of C_3S originated mainly from the reactive sites around its more ionic oxygen atoms compared with that of C_2S . Laanaiya et al. [17] conducted a density functional theory (DFT) study to analyze the ground state properties of C_3S , with an emphasis on investigating the reaction mechanism of C_3S . Apart from the structural and electronic properties of calcium silicates, the water adsorption on calcium silicates surfaces, which is often regarded as the initial step for cement hydration [18,19], has also been studied. For example, Zhang et al. [13] conducted a DFT study to reveal the single water adsorption on C_3S low-index surfaces and analyzed the electronic properties of the adsorption. Qi et al. [12] investigated the molecular and dissociative water adsorption on low-index surfaces of both β - C_2S and M3- C_3S . Other relevant studies regarding the water adsorption on calcium silicates surfaces include, but not limited to, Zhang et al. [20,21], Qi et al. [22], and Wang et al. [23]. However, the above studies mainly focus on the structural and electronic properties of pure calcium silicates, which is rarely observed in practice [7].

It is known that the most common impurities include Mg^{2+} , Al^{3+} , and Fe^{3+} , which can substitute Ca^{2+} in calcium silicates [11]. Understanding the role of impurities is vital to reveal the hydration mechanism of calcium silicates [24]. A number of studies have thus been conducted to investigate the impact of chemical impurities on the structural and electronic properties of bulk calcium silicates [11,16,25–27]. For example, Tao et al. [26] investigated the Zn incorporation into silicate clinker using DFT calculations and proposed two indicators to characterize the Zn-doping mechanism. It was found that the preference of the zinc substitution was mainly controlled by the overall crystal deformation and local structural distortion. However, the impact of chemical impurities in the water adsorption over low-index surfaces of calcium silicates has not been well studied at the atomic level using first-principles DFT calculations.

In this work, the adsorption of a single water molecule over Mg-doped low-index surfaces of calcium silicates was investigated. Bader charge analysis was performed for the selection of doping sites and the impurity formation energy (E_{for}) was calculated. The water adsorption was investigated in both a molecular and dissociative way. The adsorption energy (E_{ad}) was calculated and the adsorption configuration was analyzed. Electronic properties, i.e., Bader charge, the partial density of states (PDOS), and decomposed charge density, were studied to reveal the binding mechanism of the water molecule over Mg-doped calcium silicates surfaces. A detailed comparison was conducted on the structural and electronic properties before and after water adsorption, and the results of water adsorption over Mg-doped calcium silicates surfaces were compared with that over pristine calcium silicates surfaces.

2. Computational Methods

In this work, β - C_2S and M3- C_3S morphologies were investigated due to their frequent occurrence during industrial applications of OPC [28,29]. All first-principles DFT calculations were conducted using the projector augmented-wave (PAW) method implemented in the VASP code [30–32]. The exchange-correlation potential was approximated by the Perdew-Burke-Ernzerhof (PBE) functional within the generalized gradient approximation (GGA) [33]. Valence electrons of $3p^6 4s^2$, $3s^2$, $3s^2 3p^2$, $2s^2 2p^4$, and $1s^1$ were selected for Ca, Mg, Si, O and H, respectively. After convergence tests, the kinetic energy cutoff was determined to be 600 eV and the energy tolerance was set to be 1.0×10^{-5} eV/atom. The structural relaxation of bulk calcium silicates was conducted until the maximum residual force on each atom was smaller than 0.01 eV/Å. Interested readers can refer to our previous work [12] for a detailed discussion about the bulk structures of β - C_2S and M3- C_3S .

Starting from the relaxed unit cells, low-index surfaces were cleaved with the retaining of the in-plane crystalline periodicity. Stoichiometry and neutrality were maintained during the surface cleavage. Moreover, the SiO_4 tetrahedron is preserved since it is energetically costly to break the Si-O

covalent bond. Multiple cuts were tested to ensure the lowest energy configuration, and the slab and vacuum thicknesses were verified by convergence tests. The surface relaxation was performed without considering the symmetry between the top surface and the bottom surface [10]. Dipole correction was applied during surface calculations and the maximum residual force on each atom = 0.03 eV/Å was used as the converging criterion. For all DFT calculations, the electronic minimization was performed following the blocked Davidson iteration scheme and the ions updating was performed using the conjugate gradient algorithm. The surface energy for all low-index surfaces was calculated. Table S1 summarizes the calculation details (i.e., the Brillouin zone mesh) and the surface energy (γ) of pristine low-index surfaces of calcium silicates.

To determine the doping site of Mg, the chemical reactivity of Ca atoms was investigated. In this work, the Bader charge was calculated for surface Ca atoms since it is well regarded as an effective way to indicate surface reactivities [34,35]. The surface Ca atom with the highest chemical reactivity, namely the lowest Bader charge, was selected as the doping site of Mg. The substitution of Ca^{2+} with Mg^{2+} was performed, and then the surface slab was relaxed. The same DFT settings, i.e., energy cutoff and maximum residual force, were applied for the Mg-doped surface relaxation. The authors note that the determination of the substitution site using chemical reactivity was mainly due to the availability of computational resources. Impurity formation energy (E_{for}) was used as the indicator to understand the solubility of the dopants inside host lattice, which can be calculated as follows [36]:

$$E_{\text{for}} = E_{\text{S}}(\text{Mg}) - E_{\text{S}}(\text{pristine}) - \mu_{\text{Mg}} + \mu_{\text{Ca}} \quad (1)$$

where $E_{\text{S}}(\text{Mg})$ is the total energy of the Mg-doped slab, $E_{\text{S}}(\text{pristine})$ is the total energy of the pristine slab model, and μ_{Mg} and μ_{Ca} are the chemical potential of Mg and Ca atoms, respectively. The μ_{Mg} and μ_{Ca} were calculated from the total energy per atom in their stable structures, which were relaxed using the same DFT settings for the unit cell relaxation of calcium silicates.

Molecular water adsorption involved the placement of a free water molecule 3 Å above the Mg atom (Figure 1a). In terms of the dissociative water adsorption, one hydroxyl group was placed 3 Å above the Mg atom and the remaining proton was placed 1 Å above the adjacent dominating O atom, whose reactivity was determined by the Bader charge (Figure 1b). For the water adsorption calculations, the van der Waals correction D3 was also employed [37–39]. The adsorption energy (E_{ad}) can be obtained using the following equation:

$$E_{\text{ad}} = E_{\text{total}} - E_{\text{clean}} - E_{\text{water}} \quad (2)$$

where E_{total} is the total energy of the (water + surface) system after adsorption, E_{clean} is the total energy of the clean surface slab before adsorption, and E_{water} is the energy of an isolated H_2O in a vacuum. Thermochemically speaking, the more negative of E_{ad} , the more favorable of the adsorption.

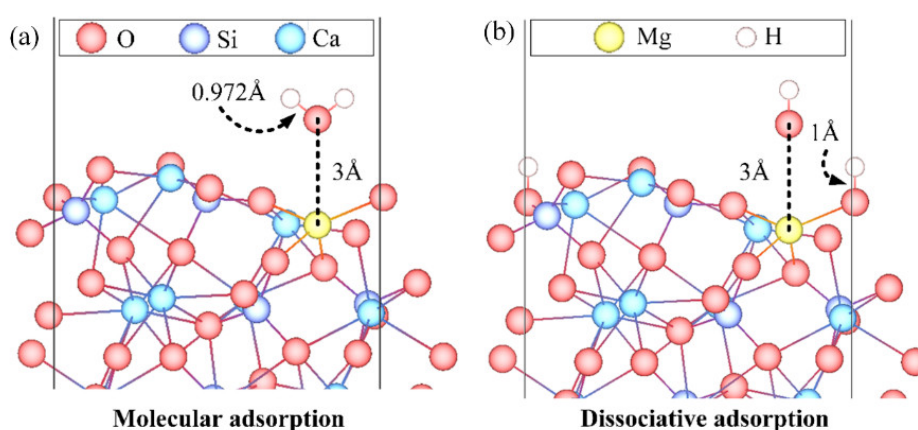


Figure 1. Initial water configuration for the (a) molecular and (b) dissociative water adsorption on the β - C_2S (100) surface (side view).

3. Computational Results

3.1. Impurity Formation Energy

Table 1 summarizes the calculated E_{for} of Mg substituting for Ca in low-index calcium silicates surfaces. Almost all cases, except Mg substitution in M3- C_3S (111) surface, were characterized by the positive E_{for} . More specifically, the E_{for} ranged from 0.51 eV to 1.21 eV for β - C_2S , with 0.51 eV being observed at (101) and (111) surfaces while 1.21 eV was observed at the (001) surface. In the case of the Mg substitution in M3- C_3S surfaces, the largest E_{for} occurred at the (101) surface (1.58 eV). A negative E_{for} of -0.02 eV, though quite small, was observed at the M3- C_3S (111) surface. From a thermodynamic point of view, a positive E_{for} means the substitution is not energetically favorable [36]. Therefore, Mg substitution was unlikely to form under thermodynamically equilibrium conditions for most low-index surfaces of calcium silicates. On the contrary, only the Mg substitution on the M3- C_3S (111) surface was marginally favorable in energy.

Table 1. Impurity formation energy (E_{for}) of Mg substituting for Ca in low-index calcium silicates surfaces.

Calcium Silicate Phase	Low-Index Surfaces	E_{for} (eV)	Calcium Silicate Phase	Low-Index Surfaces	E_{for} (eV)
β - C_2S	(100)	0.82	M3- C_3S	(100)	0.46
	(010)	0.74		(010)	0.53
	(001)	1.21		(001)	0.76
	(110)	0.78		(110)	0.19
	(101)	0.51		(101)	1.58
	(011)	0.94		(011)	0.48
	(111)	0.51		(111)	-0.02

3.2. Adsorption Energy

In this section, we present our theoretical results for the E_{ad} of the H_2O over Mg-doped surfaces of β - C_2S and M3- C_3S . The calculated E_{ad} are listed in Table 2.

Table 2. E_{ad} (eV) of a single H₂O over Mg-doped surfaces of β -C₂S and M3-C₃S.

β -C ₂ S	Dissociated	Free	M3-C ₃ S	Dissociated	Free
(100)	−1.249 (D)		(100)	−1.624 (D)	−0.699 (M)
(010)	−0.869 (D)	−0.937 (M)	(010)	−1.786 (D)	−0.938 (M)
(001)	−0.994 (M)	−0.915 (M)	(001)	−1.708 (D)	−0.868 (M)
(110)	−0.952 (M)		(110)	−3.028 (D)	−1.089 (M)
(101)	−0.765 (M)	−0.831 (M)	(101)	−4.008 (D)	−2.711 (D)
(011)	−0.598 (D)	−1.116 (M)	(011)	−2.192 (D)	
(111)	−0.982 (M)	−0.817 (M)	(111)	−1.454 (D)	

Note: Dissociated and free represent the initial configuration of the H₂O, M, and D in the brackets represent molecular and dissociative adsorption, respectively, after relaxation.

For the H₂O adsorption over β -C₂S surfaces, the E_{ad} ranged between −1.249 eV (dissociative adsorption on <100> surface) and −0.598 eV (dissociative adsorption on <011> surface). The hydroxyl group and the proton approached each other and formed a water molecule on β -C₂S (001), (110), (101), and (111) surfaces. In contrast, dissociation of the H₂O was only observed over the β -C₂S (100) surface. Although the dissociative adsorption over the β -C₂S (100) surface was found to be the most energetically favorable, molecular adsorption was generally more favorable considering the E_{ad} of other β -C₂S surfaces.

Though molecular adsorption was observed for the adsorption of water on β -C₂S (001), (101), and (111) surfaces regardless of the initial water configuration, the final adsorption configuration was different. Figure S1 illustrates the final adsorption configuration on the β -C₂S (001) surface as an example. The difference in the adsorption configuration led to the difference in the E_{ad} .

Dissociative water adsorption was found to be more energetically favorable than molecular water adsorption over M3-C₃S surfaces. The most negative E_{ad} (−4.008 eV) was obtained at the dissociative adsorption over the M3-C₃S (101) surface while the least negative E_{ad} (−0.699 eV) was obtained at the molecular adsorption over the M3-C₃S (100) surface. The dissociation of the H₂O was observed at M3-C₃S (101), (011), and (111) surfaces while no reformations of H₂O from the hydroxyl group and the proton were observed. The above results imply the dissociative adsorption was more stable and energetically favorable on M3-C₃S surfaces, which agrees well with the results in the literature [12,22]. Moreover, the E_{ad} of M3-C₃S surfaces was much more negative than that of β -C₂S surfaces, indicating the H₂O adsorption on M3-C₃S surfaces was stronger than that on β -C₂S surfaces.

3.3. Adsorption Configuration

Table 3 summarizes the adsorption configuration of the H₂O over β -C₂S surfaces. In most cases, bonding was found between the surface Mg atom and the O atom from the water molecule (O_w). The O_w was attracted to surface Ca atoms in the molecular adsorption on (011) and (111) surfaces, indicating the Ca-O_w bond was more favorable than the Mg-O_w bond in these two cases. Both Ca-O_w and Mg-O_w bonds can be formed simultaneously for dissociative adsorption, which was not observed during the molecular adsorption.

Table 3. Adsorption configurations of the H₂O over Mg-doped β-C₂S surfaces with respect to the adsorption energy in eV.

Surfaces	Summary of Bonding
(100)	-1.249D : Mg-O _w , Ca-O _w , O _s -H _d , O _w -H _d
(010)	-0.869D : Mg-O _w , O _s -H _d , O _w -H _d ; -0.937M : Mg-O _w , O _s -H
(001)	-0.994M and -0.915M : Mg-O _w , O _s -H
(110)	-0.952M : Mg-O _w , O _s -H
(101)	-0.765M and -0.831M : Mg-O _w , O _s -H
(011)	-0.598D : Mg-O _w , Ca-O _w (2), O _s -H _d , O _s -H _d ; -1.116M : Ca-O _w
(111)	-0.982M : Ca-O _w , O _s -H(2); -0.817M : Ca-O _w , O _s -H

Note: abbreviations in bold represent the adsorption energy (the number) and adsorption type (D stands for dissociative and M stands for molecular); O_w represents O atoms from the water molecule, O_s represents surface O atoms, H_d represents the dissociated proton, '-' represents bonds formation, '-' represents the two atoms are attracted to each without bond formation; the hydroxyl group from the water molecule is not shown for clarity.

The dissociated proton (H_d) was attracted to a surface O atom (O_s) of the calcium silicates. Moreover, the dissociative configuration was also influenced by O_w and O_s atoms. Although the adsorption configuration was mainly influenced by the Ca-O_w or the Mg-O_w bond for the molecular adsorption, the attraction between O_s and H was also crucial, such as on β-C₂S (010) and (111) surfaces.

Table 4 summarizes the adsorption configuration of the single water molecule on M3-C₃S surfaces. As shown, the dissociative adsorption was mainly characterized by the Ca-O_w bond, the Mg-O_w bond, the O_s-H_d bond, or was influenced by the attraction between O_s and H_d. In contrast, the configuration of the molecular adsorption was influenced by the Mg-O_w bond, and in some cases such as (010) and (001), also influenced by the attraction between O_s and H. The adsorption configurations for the most energetically favorable dissociative and molecular adsorptions are illustrated in Figure 2 as an example.

3.4. Partial Density of States

To reveal the bonding mechanism between the water molecule and surfaces, the partial density of states (PDOS) of atoms involved in the fresh-bond formation was analyzed. Figure 3a illustrates the bonding associated with the O_w atom during the dissociative adsorption over the β-C₂S (100) surface. O_w 2p orbital overlapped with Ca 4s and Ca 3p orbitals near the Fermi energy during the O_w-Ca bond formation. Similarly, overlapping was observed between O_w 2p orbital and Mg 3s orbital for the O_w-Mg bond. It is noted that the O_w 2p orbital also overlapped marginally with H_d 1s orbital, indicating the O_w and H_d were attracted to each other.

Table 4. Adsorption configurations of the H₂O over Mg-doped M3-C₃S surfaces with respect to the adsorption energy in eV.

Surfaces	Summary of Bonding
(100)	-1.624D : Mg-O _w , Ca-O _w (2), O _s -H _d ; -0.699M : Mg-O _w
(010)	-1.786D : Mg-O _w , Ca-O _w , O _s -H _d ; -0.938M : Mg-O _w , O _s -H
(001)	-1.708D : Mg-O _w , Ca-O _w (2), O _s -H _d , O _w -H _d ; -0.868M : Mg-O _w , O _s -H
(110)	-3.028D : Mg-O _w , Ca-O _w , O _s -H _d , O _s -H _d ; -1.089M : Mg-O _w
(101)	-4.008D : Mg-O _w , Ca-O _w , O _s -H _d ; -2.711D : Mg-O _w , Ca-O _w (2), O _s -H _d
(011)	-2.192D : Mg-O _w , Ca-O _w , O _s -H _d , O _w -H _d
(111)	-1.454D : Ca-O _w , O _s -H _d , O _w -H _d

Note: abbreviations are explained in Table 3.

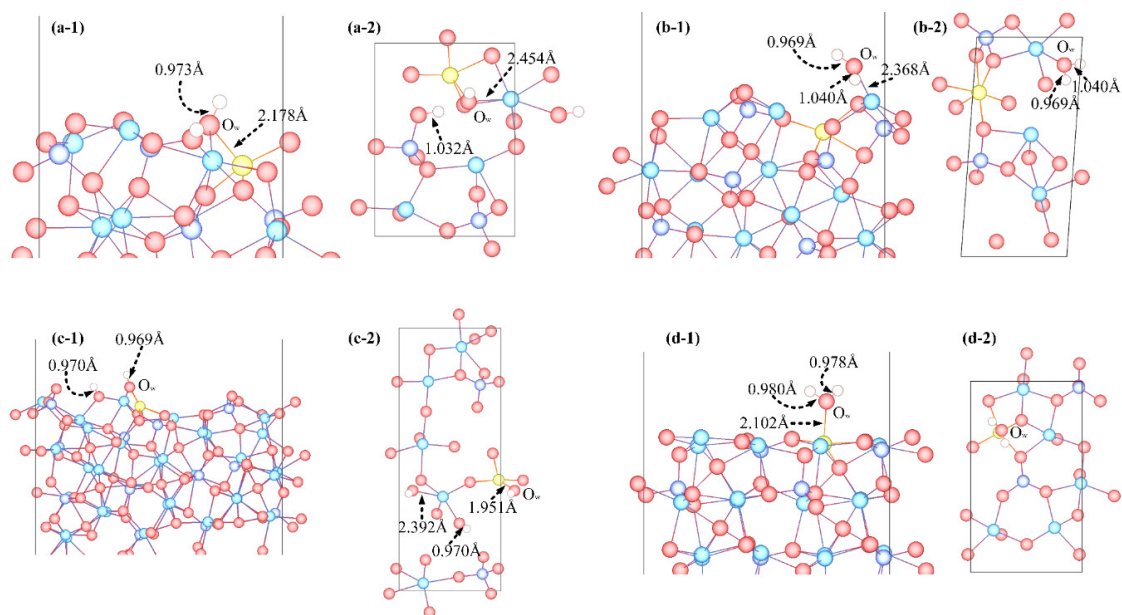


Figure 2. Water adsorption configuration of: (a) dissociative adsorption on the β -C₂S (100) surface, (b) molecular adsorption on the β -C₂S (011) surface, (c) dissociative adsorption on the M3-C₃S (101) surface, and (d) molecular adsorption on the M3-C₃S (100) surface. Note: 1—side view and 2—top view.

The O_s-H_d bonding was mainly originated from the overlapping between O_s 2*p* and H_d 1*s* orbitals (Figure 3b). Moreover, O_s 2*s* orbital overlapped marginally with H_d 1*s* orbital at around −5 eV. In the case of the molecular adsorption over β -C₂S (011) surface, the orbital overlapping was similar to that during the dissociative adsorption, which was the O_w 2*p* orbital overlapping with Ca 4*s* and Ca 3*p* orbitals (Figure 3c). Similar orbital overlapping was observed during the water adsorption on other low-index surfaces of calcium silicates.

To summarize, the O_w-Mg bonding originated from the overlapping between O_w 2*p* orbital and Mg 3*s* orbital, the O_w-Ca bonding originated from the overlapping between O_w 2*p* orbital and Ca 4*s*/3*p* orbitals, and the O_s-H_d bonding mainly originated from the overlapping between O_s 2*p* and H_d 1*s* orbitals. The authors note that the PDOS results might show some difference with the results in the literature, such as in [40] and [27], due to the difference in DFT computational settings. Moreover, the PDOS near the conduction band minimum was not discussed since the overlapping was not as significant as that near the valence band maximum.

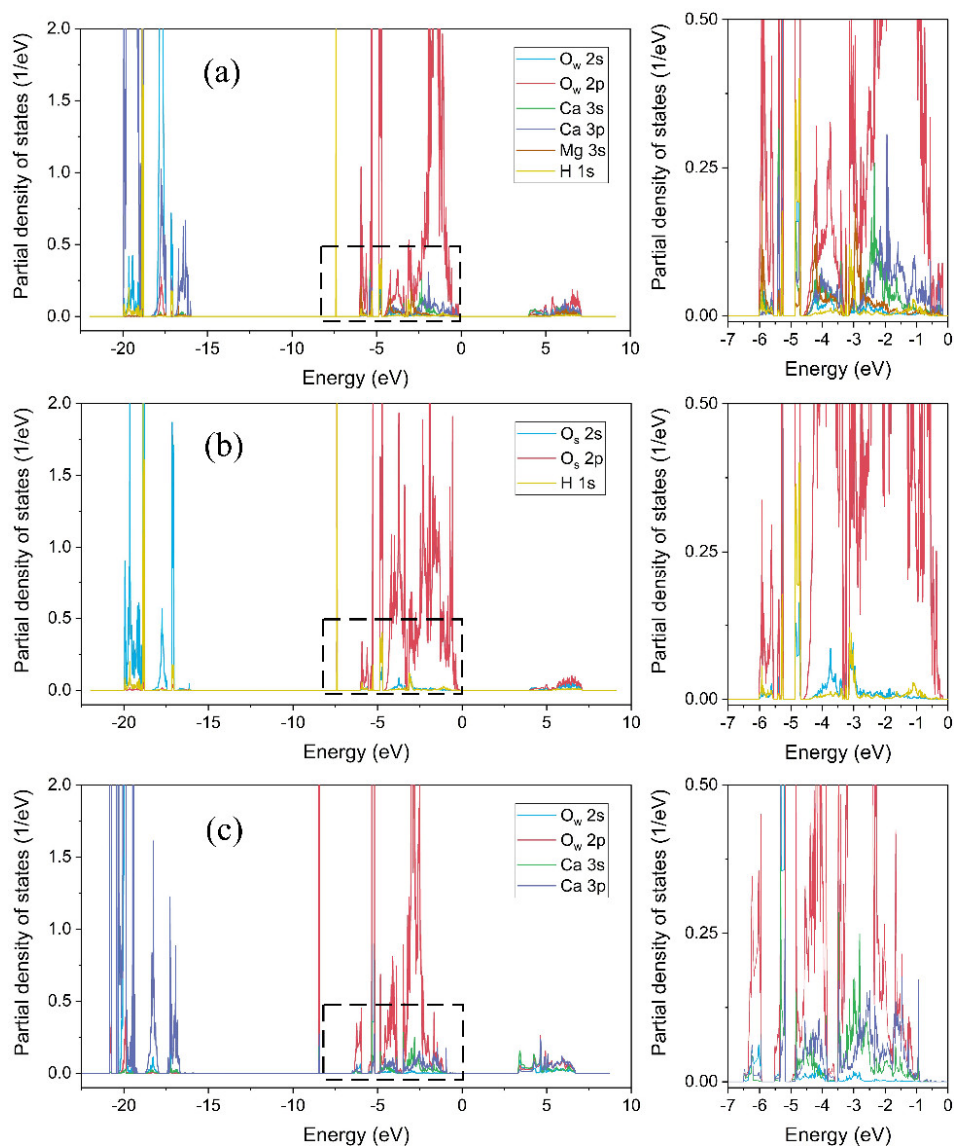


Figure 3. Partial density of states (PDOS) of the water adsorption on the Mg-doped β -C₂S (100) and (011) surfaces: (a) dissociative adsorption on the Mg-doped β -C₂S (100) surface-O_w bonding, (b) dissociative adsorption on the Mg-doped β -C₂S (100) surface-H_d bonding, and (c) molecular adsorption on Mg-doped β -C₂S (011) surface. Note: right sub-figures are enlarged representations of regions in the box and the Fermi energy was set at 0.00 eV.

4. Discussion

4.1. What Does the Positive E_{for} Imply?

As indicated in Table 1, the E_{for} of Mg substituting for Ca was positive for most cases, indicating such a substitution was energetically unfavorable. However, Mg substitution in the current study was only used to investigate the influence of Mg substitution on water adsorption. In reality, the Mg substitution occurs in the solid solution during the cement production. Under such circumstances, the raw materials are heated up to 1400 °C [7,41], which can promote the Mg substitution in bulk and at the surface.

Moreover, the main objective of Mg substitution is in the polymorphic modification. A higher proportion of MgO during C₃S crystallization stabilizes the M3 phase [7]. In the case of C₂S, Chan et al. [42]

found that the ionic substitution is vital in stabilizing the polymorphic form of C_2S other than γ , the only stable form at room temperature without impurities [7].

4.2. Comparison before and after Water Adsorption

In this section, the change of structural and electronic properties of low-index surfaces after water adsorption is analyzed. Figure 4 illustrates the bond length distribution of surface Mg-O before and after water adsorption. An increase in surface Mg-O bond length was observed after water adsorption, indicating the weakening of surface Mg-O bonds [12]. More specifically, the average Mg-O bond was increased by 0.007 Å after the dissociative water adsorption over β - C_2S low-index surfaces. In contrast, the average Mg-O bond was increased by 0.043 Å after the molecular water adsorption over β - C_2S low-index surfaces. The above results imply the molecular adsorption could weaken the surface Mg-O bond to a larger extent for β - C_2S surfaces.

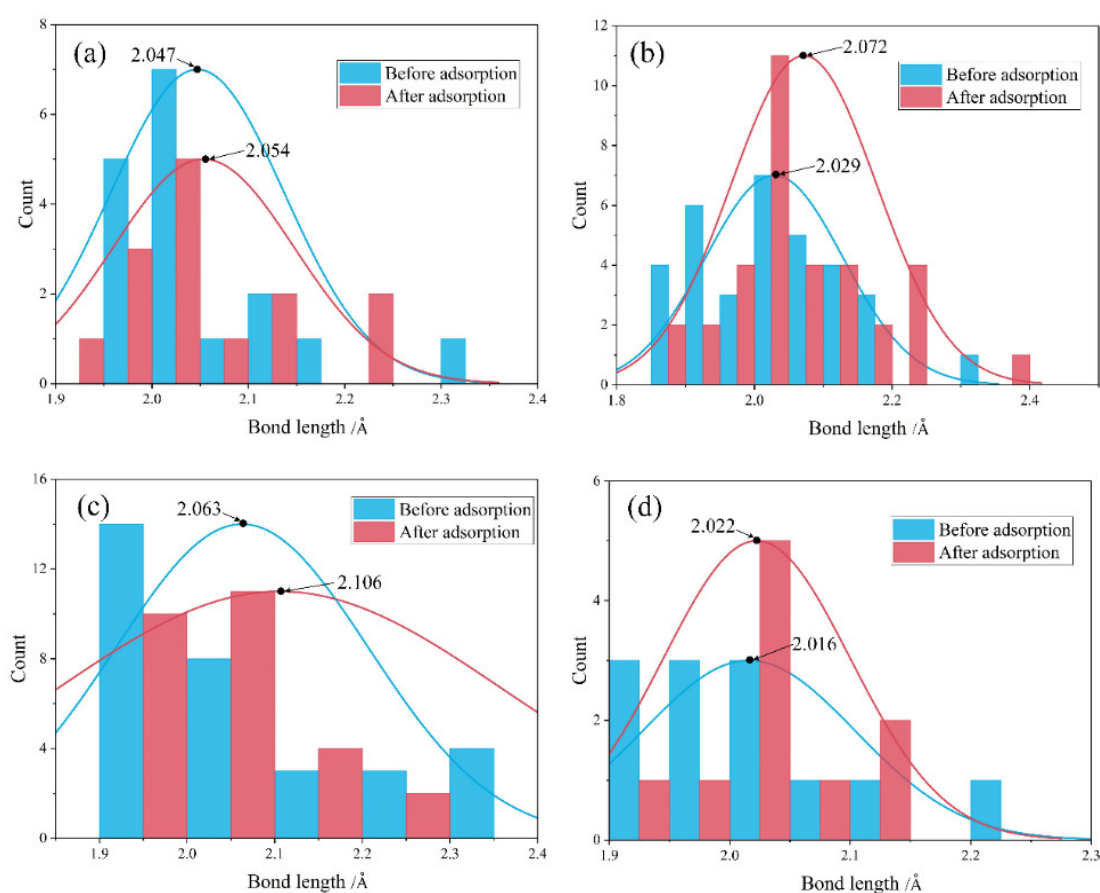


Figure 4. Distribution of surface Mg-O bond length that was involved in water adsorption: (a) dissociative adsorption on β - C_2S surfaces, (b) molecular adsorption on β - C_2S surfaces, (c) dissociative adsorption on $M3-C_3S$ surfaces, and (d) molecular adsorption on $M3-C_3S$ surfaces.

In the case of the Mg-O bond length on $M3-C_3S$ surfaces, a 0.043 Å and 0.006 Å increase was found for the dissociative adsorption and molecular adsorption, respectively. Dissociative adsorption was better at weakening surface Mg-O bonds than molecular adsorption for $M3-C_3S$ surfaces. Since the weakening of surface bonds implies the increasing probability of bond breakage, the dissolution of Mg was promoted after the water adsorption [22]. Furthermore, molecular adsorption is more beneficial to Mg dissolution in β - C_2S surfaces while dissociative adsorption is more beneficial to Mg dissolution in $M3-C_3S$ surfaces.

Figure 5 illustrates the effect of water adsorption on the Bader charge of surface atoms that were involved in the bond formation. As shown, the Bader charge of surface Mg, Ca, and O_s increased after water adsorption, indicating a decrease of electrons. In contrast, the O_w and H_d accepted electrons, resulting in a decrease of the Bader charge. Taking β-C₂S as an example, the Bader charge of Mg, Ca, and O_s was increased from 1.665 eV, 1.564 eV, and −1.590 eV, respectively, to 1.670 eV, 1.585 eV, and −1.495 eV. The above results indicate that the electron is transferred from the surface to the H₂O upon adsorption, which agrees well with the results in the literature [12,13,22].

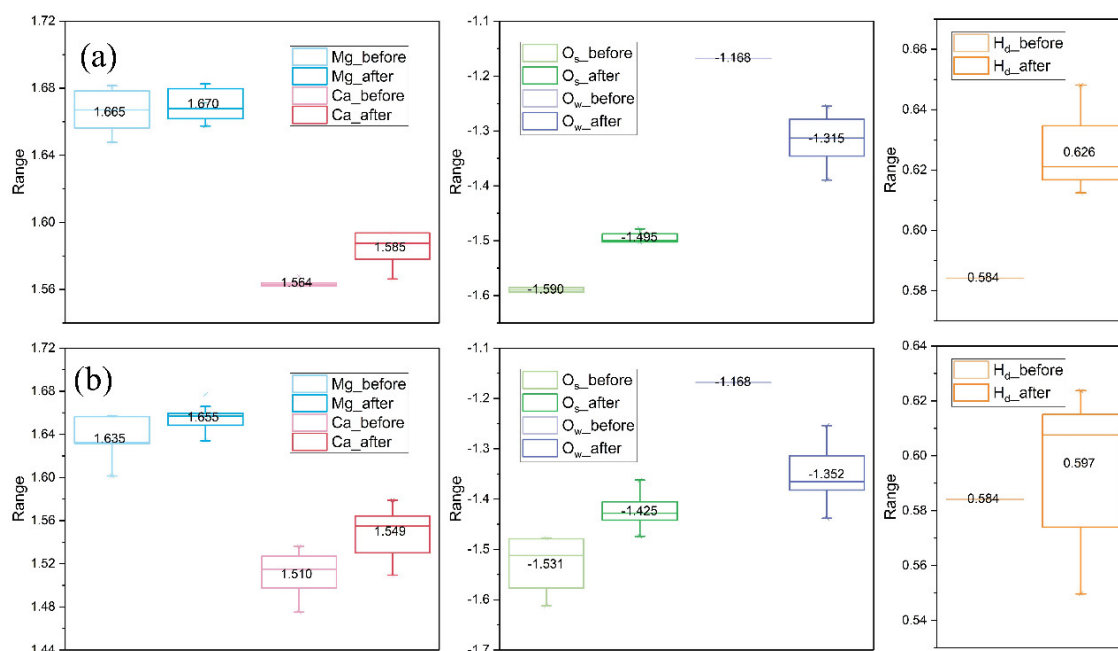


Figure 5. The influence of water adsorption on the Bader charge of surface atoms that were involved in the bond formation: (a) β-C₂S surfaces, and (b) M3-C₃S surfaces. Note: numbers in the box are mean values.

The electron transfer can also be indicated by the decomposed charge density. In the current study, the decomposed charge density distribution around the top of the valence band (ρ_{TVB} , −6 eV to 0 eV) and around the bottom of the conduction band (ρ_{BCB} , 0 to 3 eV) was analyzed before and after water adsorption. Figure 6 illustrates the results of the molecular adsorption over the β-C₂S (011) surface as an example. The ρ_{TVB} and ρ_{BCB} of surface and water atoms were changed during the water adsorption. The comparison between the density of ρ_{TVB} and ρ_{BCB} before and after adsorption indicates the electron transfer from the surface to the H₂O.

4.3. Comparison with Pristine Low-Index Surfaces of Calcium Silicates

In this section, the Mg-doped surfaces are compared with pristine surfaces to reveal the role of Mg doping in the water adsorption over calcium silicate surfaces. As shown in Figure 5, the average Bader charge of Mg in β-C₂S surfaces and M3-C₃S surfaces was 1.665 eV and 1.635 eV, respectively. Compared with the Bader charge of surface Ca atoms (around 1.5 eV as shown in Figure 5 and in the literature [12]), the Mg site might be less reactive than the corresponding Ca site. The reactivity of surface Mg and Ca sites can also be revealed by the decomposed charge density. It can be seen from Figure 6c that the ρ_{BCB} was mainly distributed around surface Ca atoms, implying the surface Ca atoms were more reactive than surface Mg atoms under nucleophilic attack.

Figure 7 illustrates the comparison of the E_{ad} of the single water adsorption on pristine and Mg-doped β-C₂S and M3-C₃S surfaces. Generally speaking, the E_{ad} became less negative after the Mg impurity (lighter color in the upper two rows compared with the lower two rows, as shown in

Figure 7). In the case of $\beta\text{-C}_2\text{S}$ (100), $\beta\text{-C}_2\text{S}$ (001), $\text{M3-C}_3\text{S}$ (101), and $\text{M3-C}_3\text{S}$ (011) surfaces, the E_{ad} became more negative.

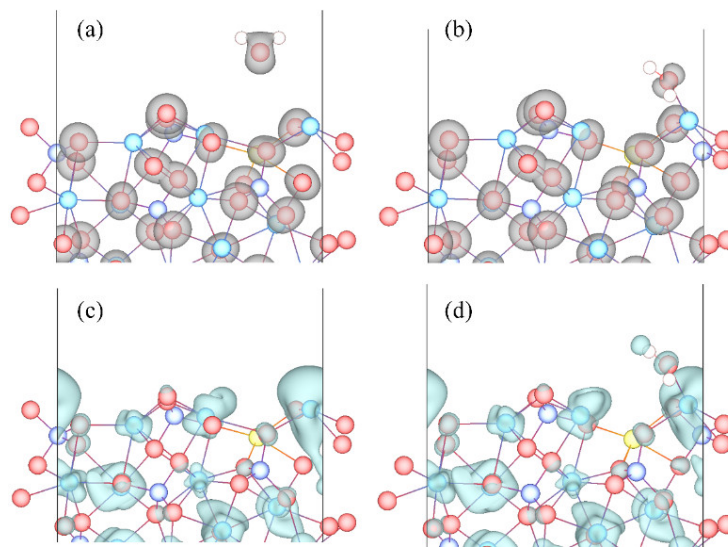


Figure 6. Decomposed charge density of the molecular adsorption on the $\beta\text{-C}_2\text{S}$ (011) surface: (a) ρ_{TVB} before adsorption, (b) ρ_{TVB} after adsorption, (c) ρ_{BCB} before adsorption, and (d) ρ_{BCB} after adsorption. Note: isosurface level was 0.05 eV for ρ_{TVB} illustration and 0.02 eV for ρ_{BCB} illustration.

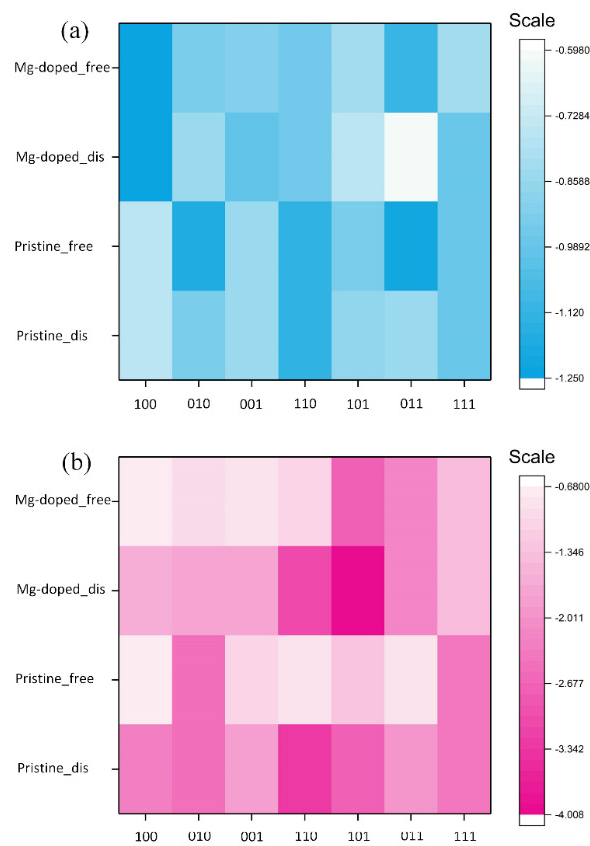


Figure 7. Comparison of E_{ad} of a single water molecule on pristine and Mg-doped surfaces of: (a) $\beta\text{-C}_2\text{S}$, and (b) $\text{M3-C}_3\text{S}$. Note: the dis and free in the y-axis represents dissociated water and free water in the initial configuration.

The authors note that the more negative E_{ad} after Mg impurity on β - C_2S (100), β - C_2S (001), M3- C_3S (101), and M3- C_3S (011) surfaces is not due to the Mg- O_w bonding was more energetically favorable than Ca- O_w . Instead, more bonds were formed on these Mg-doped surfaces. More specifically, the coexistence of Mg- O_w and Ca- O_w bonds, as well as the attraction between H and O_s even for the molecular adsorption, led to the more negative E_{ad} .

The influence of Mg doping on the water adsorption can also be indicated by the water configuration. For one thing, the water adsorption could be influenced by the adjacent Ca site to a larger extent on the Mg-doped surfaces than the pristine surfaces. In some cases, the water molecule is absorbed into the adjacent Ca site even if it is placed above the Mg site in its initial configuration (Figure 2b). Figure 8 illustrates the difference between the dissociative adsorption configuration over the M3- C_3S (111) surface. As shown, the O_w was attracted to one adjacent Ca site on the Mg-doped surface, instead of shared by three Ca sites on the pristine surface. The reason for such a difference in adsorption configuration is due to the relatively low reactivity of the Mg site, as discussed in Section 4.1. Therefore, the adjacent Ca site could be much more reactive compared with the Mg site, resulting in the water adsorption around the adjacent Ca site.

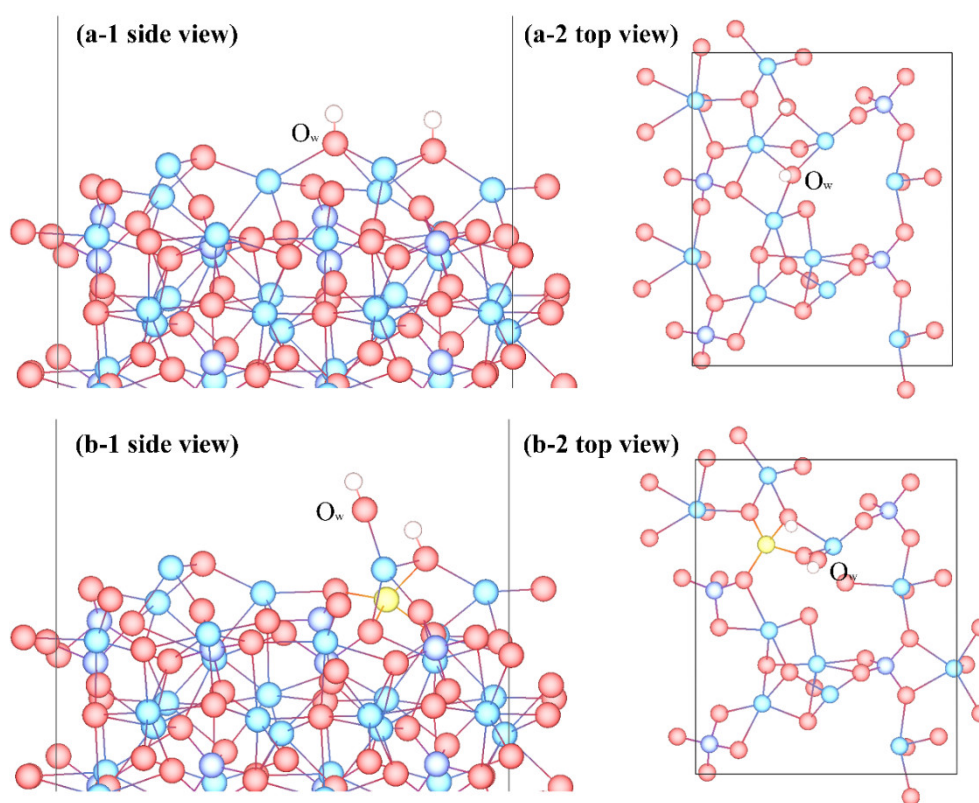


Figure 8. The dissociative adsorption configuration on the M3- C_3S (111) surface of: (a) pristine surface, and (b) Mg-doped surface.

Another influence of Mg doping on the adsorption configuration could be revealed by comparing Tables 3 and 4 with Table 6 in the literature [12]. As shown, water reformation from H^+ and OH^- was not as frequently observed on Mg-doped β - C_2S surfaces than on those pristine ones. On the pristine β - C_2S surfaces, water reformation was observed on most surfaces, except the (011) surface. However, such water reformations were not observed on the (100), (010), and (011) Mg-doped surfaces. Moreover, water dissociation occurred on the β - C_2S Mg-doped (100) surface, which was not observed on the pristine surface. The frequency of water dissociation on M3- C_3S was quite similar on pristine and Mg-doped surfaces, even though occurring at different surfaces. The water reformation and dissociation are influenced by the relaxed surface structure, which in turn affect the energy barrier for

such a process. Thus, a detailed discussion about the influence of Mg doping on the water reformation and dissociation would require further calculations and analysis.

5. Conclusions

In this work, using first-principles DFT calculations, we investigated the influence of Mg doping on the water adsorption over calcium silicates surfaces. Both molecular and dissociative adsorption were analyzed, and the influence of water adsorption was investigated. A detailed comparison between Mg-doped and pristine surfaces, both in terms of surface structures and water adsorption, was conducted. The following conclusions can be summarized based on the calculated results:

1. The E_{for} of Mg substituting for Ca ranged 0.51 to 1.21 eV on β -C₂S surfaces and −0.02 to 1.58 eV on M3-C₃S surfaces.
2. The E_{ad} of an H₂O over Mg-doped surfaces of β -C₂S and M3-C₃S ranged from −0.598 to −1.249 eV and −0.699 to −4.008 eV, respectively. Generally speaking, molecular adsorption was more energetically favorable on β -C₂S surfaces and dissociative adsorption was more favorable on M3-C₃S surfaces.
3. Molecular adsorption was characterized by the Mg-O_w bond and/or the Ca-O_w bond, and in some cases, was also influenced by the attraction between O_s and H. Dissociative adsorption was mainly characterized by the Ca-O_w bond, Mg-O_w bond, O_s-H_d bond, or was influenced by the attraction between O_s and H_d.
4. O_w-Mg bonds were originated from the O_w 2*p* orbital and the Mg 3*s* orbital, O_w-Ca bonds were originated from the O_w 2*p* orbital and the Ca 4*s*/3*p* orbitals, and O_s-H_d bonds was mainly originated from the O_s 2*p* and the H_d 1*s* orbitals.
5. Water adsorption increased the bond length of surface Mg-O and promoted the Mg dissolution. Such a bond-weakening effect was more evident for the molecular adsorption over β -C₂S surfaces and the dissociative adsorption over M3-C₃S surfaces. The electron transfer was observed from the surface to H₂O upon adsorption.
6. Mg doping influenced the reactivity of surface Ca/Mg sites, the E_{ad} of the single water adsorption, as well as the adsorption configuration compared with the water adsorption on pristine surfaces.

In the future, the influence of Mg concentration on the water adsorption should be investigated. Moreover, a systematic study should be performed to determine the substitution site for more representative results. Finally, more adsorption sites could be investigated to better reveal the influence of Mg substitution on the water adsorption.

Supplementary Materials: The following are available online at <http://www.mdpi.com/2075-163X/10/8/665/s1>, Figure S1: Water adsorption configuration on β -C₂S (001) surface: (a) −0.994 eV, and (b) −0.915 eV. Please refer to Figure 1 for the atom type, Table S1: Calculation details and the surface energy of pristine low-index surfaces of calcium silicates.

Author Contributions: Conceptualization, C.Q. and Q.C.; methodology, C.Q.; software, C.Q.; validation, A.F. and Q.C.; formal analysis, A.F.; writing—original draft preparation, C.Q.; writing—review and editing, Q.C. and A.F.; funding acquisition, Q.C. All authors have read and agreed to the published version of the manuscript.

Funding: This work was supported by resources provided by the Pawsey Supercomputing Centre (No. PAWSEY0308) with funding from the Australian Government and the Government of Western Australia, the State Key Laboratory of Safety and Health for Metal Mines (No.2019-JSKSSYS-02), and Natural Science Foundation of Hunan Province, China (No. 2020JJ5718).

Conflicts of Interest: There is no conflict of interest to declare.

References

1. Singh, S.K.; Singh, A.; Singh, B.; Vashistha, P. Application of thermo-chemically activated lime sludge in production of sustainable low clinker cementitious binders. *J. Clean. Prod.* **2020**, *264*, 121570. [CrossRef]
2. Wang, D.L.; Zhang, Q.L.; Chen, Q.S.; Qi, C.C.; Feng, Y.; Xiao, C.C. Temperature variation characteristics in flocculation settlement of tailings and its mechanism. *Int. J. Miner. Metall. Mater.* **2020**. [CrossRef]

3. Feng, Y.; Chen, Q.; Zhou, Y.; Yang, Q.; Zhang, Q.; Jiang, L.; Guo, H. Modification of glass structure via CaO addition in granulated copper slag to enhance its pozzolanic activity. *Constr. Build. Mater.* **2020**, *240*, 117970. [[CrossRef](#)]
4. Chen, X.; Shi, X.; Zhou, J.; Yu, Z.; Huang, P. Determination of mechanical, flowability, and microstructural properties of cemented tailings backfill containing rice straw. *Constr. Build. Mater.* **2020**, *246*, 118520. [[CrossRef](#)]
5. Chen, X.; Shi, X.; Zhang, S.; Chen, H.; Zhou, J.; Yu, Z.; Huang, P. Fiber-Reinforced Cemented Paste Backfill: The Effect of Fiber on Strength Properties and Estimation of Strength Using Nonlinear Models. *Materials* **2020**, *13*, 718. [[CrossRef](#)] [[PubMed](#)]
6. Tao, Y.; Zhang, W.; Li, N.; Wang, F.; Hu, S. Atomic occupancy mechanism in brownmillerite $\text{Ca}_2\text{FeAlO}_5$ from a thermodynamic perspective. *J. Am. Ceram. Soc.* **2019**, *103*, 635–644. [[CrossRef](#)]
7. Taylor, H.F.W. *Cement Chemistry*, 2nd ed.; Thomas Telford Publishing: London, UK, 1997.
8. Qi, C.; Fourie, A.; Chen, Q.; Liu, P.-F. Application of first-principles theory in ferrite phases of cemented paste backfill. *Miner. Eng.* **2019**, *133*, 47–51. [[CrossRef](#)]
9. Huang, J.; Valenzano, L.; Singh, T.V.; Pandey, R.; Sant, G. Influence of (Al, Fe, Mg) Impurities on Triclinic Ca_3SiO_5 : Interpretations from DFT Calculations. *Cryst. Growth Des.* **2014**, *14*, 2158–2171. [[CrossRef](#)]
10. Durgun, E.; Manzano, H.; Kumar, P.V.; Grossman, J.C. The Characterization, Stability, and Reactivity of Synthetic Calcium Silicate Surfaces from First Principles. *J. Phys. Chem. C* **2014**, *118*, 15214–15219. [[CrossRef](#)]
11. Manzano, H.; Durgun, E.; Qomi, M.J.A.; Ulm, F.-J.; Pellenq, R.J.M.; Grossman, J.C. Impact of Chemical Impurities on the Crystalline Cement Clinker Phases Determined by Atomistic Simulations. *Cryst. Growth Des.* **2011**, *11*, 2964–2972. [[CrossRef](#)]
12. Qi, C.; Spagnoli, D.; Fourie, A. DFT-D study of single water adsorption on low-index surfaces of calcium silicate phases in cement. *Appl. Surf. Sci.* **2020**, *518*, 146255. [[CrossRef](#)]
13. Zhang, Y.; Lu, X.; Song, D.; Liu, S. The adsorption of a single water molecule on low-index C3S surfaces: A DFT approach. *Appl. Surf. Sci.* **2019**, *471*, 658–663. [[CrossRef](#)]
14. Manzano, H.; Durgun, E.; López-Arbeloa, I.; Grossman, J.C. Insight on Tricalcium Silicate Hydration and Dissolution Mechanism from Molecular Simulations. *ACS Appl. Mater. Interfaces* **2015**, *7*, 14726–14733. [[CrossRef](#)] [[PubMed](#)]
15. Wang, Q.; Manzano, H.; Guo, Y.; López-Arbeloa, I.; Shen, X. Hydration Mechanism of Reactive and Passive Dicalcium Silicate Polymorphs from Molecular Simulations. *J. Phys. Chem. C* **2015**, *119*, 19869–19875. [[CrossRef](#)]
16. Durgun, E.; Manzano, H.; Pellenq, R.J.M.; Grossman, J.C. Understanding and Controlling the Reactivity of the Calcium Silicate phases from First Principles. *Chem. Mater.* **2012**, *24*, 1262–1267. [[CrossRef](#)]
17. Laanaiya, M.; Bouibes, A.; Zaoui, A. Understanding why Alite is responsible of the main mechanical characteristics in Portland cement. *Cem. Concr. Res.* **2019**, *126*, 105916. [[CrossRef](#)]
18. Dovál, M.; Palou, M.; Mojumdar, S.C. Hydration behavior of C2S and C2AS nanomaterials, synthesized by sol-gel method. *J. Therm. Anal. Calorim.* **2006**, *86*, 595–599. [[CrossRef](#)]
19. Thissen, P.; Natzeck, C.; Giraudo, N.; Weidler, P.; Wöll, C. Hydration of Concrete: The First Steps. *Chem. A Eur. J.* **2018**, *24*, 8603–8608. [[CrossRef](#)]
20. Zhang, Y.; Lu, X.; He, Z.; Song, D. Molecular and dissociative adsorption of a single water molecule on a β -dicalcium silicate (100) surface explored by a DFT approach. *J. Am. Ceram. Soc.* **2017**, *101*, 2428–2437. [[CrossRef](#)]
21. Zhang, Y.; Lu, X.; Song, D.; Liu, S. The Adsorption Behavior of a Single and Multi-Water Molecules on Tricalcium Silicate (111) Surface from DFT Calculations. *J. Am. Ceram. Soc.* **2018**, *102*, 2075–2083. [[CrossRef](#)]
22. Qi, C.; Liu, L.; He, J.; Chen, Q.; Yu, L.-J.; Liu, P.-F. Understanding Cement Hydration of Cemented Paste Backfill: DFT Study of Water Adsorption on Tricalcium Silicate (111) Surface. *Minerals* **2019**, *9*, 202. [[CrossRef](#)]
23. Wang, Q.; Manzano, H.; López-Arbeloa, I.; Shen, X. Water Adsorption on the β -Dicalcium Silicate Surface from DFT Simulations. *Minerals* **2018**, *8*, 386. [[CrossRef](#)]
24. Huang, J.; Wang, B.; Yu, Y.; Valenzano, L.; Bauchy, M.; Sant, G. Electronic Origin of Doping-Induced Enhancements of Reactivity: Case Study of Tricalcium Silicate. *J. Phys. Chem. C* **2015**, *119*, 25991–25999. [[CrossRef](#)]
25. Saritas, K.; Ataca, C.; Grossman, J.C. Predicting Electronic Structure in Tricalcium Silicate Phases with Impurities Using First-Principles. *J. Phys. Chem. C* **2015**, *119*, 5074–5079. [[CrossRef](#)]

26. Tao, Y.; Li, N.; Zhang, W.; Wang, F.; Hu, S. Understanding the zinc incorporation into silicate clinker during waste co-disposal of cement kiln: A density functional theory study. *J. Clean. Prod.* **2019**, *232*, 329–336. [[CrossRef](#)]
27. Tao, Y.; Zhang, W.; Shang, D.; Xia, Z.; Li, N.; Ching, W.-Y.; Wang, F.; Hu, S. Comprehending the occupying preference of manganese substitution in crystalline cement clinker phases: A theoretical study. *Cem. Concr. Res.* **2018**, *109*, 19–29. [[CrossRef](#)]
28. De Noirfontaine, M.-N.; Dunstetter, F.; Courtial, M.; Gasecki, G.; Signes-Frehel, M. Polymorphism of tricalcium silicate, the major compound of Portland cement clinker. *Cem. Concr. Res.* **2006**, *36*, 54–64. [[CrossRef](#)]
29. Fukuda, K.; Ito, S. Improvement in Reactivity and Grindability of Belite-Rich Cement by Remelting Reaction. *J. Am. Ceram. Soc.* **1999**, *82*, 2177–2180. [[CrossRef](#)]
30. Kresse, G.; Furthmüller, J. Efficiency of ab-initio total energy calculations for metals and semiconductors using a plane-wave basis set. *Comput. Mater. Sci.* **1996**, *6*, 15–50. [[CrossRef](#)]
31. Kresse, G.; Furthmüller, J. Efficient iterative schemes for ab initio total-energy calculations using a plane-wave basis set. *Phys. Rev. B Condens. Matter Mater. Phys.* **1996**, *54*, 11169–11186. [[CrossRef](#)]
32. Kresse, G.; Hafner, J. Ab initio molecular dynamics for liquid metals. *Phys. Rev. B* **1993**, *47*, 558–561. [[CrossRef](#)] [[PubMed](#)]
33. Perdew, J.P.; Burke, K.; Ernzerhof, M. Generalized Gradient Approximation Made Simple. *Phys. Rev. Lett.* **1996**, *77*, 3865–3868. [[CrossRef](#)] [[PubMed](#)]
34. Bader, R.F.W. A quantum theory of molecular structure and its applications. *Chem. Rev.* **1991**, *91*, 893–928. [[CrossRef](#)]
35. Tang, W.; Sanville, E.; Henkelman, G. A grid-based Bader analysis algorithm without lattice bias. *J. Phys. Condens. Matter* **2009**, *21*, 084204. [[CrossRef](#)]
36. Mahmoodi, T.; Mansouri, M. Structural effects of substitutional impurities on MoO₃ bilayers: A first principles study. *J. Korean Phys. Soc.* **2016**, *69*, 1439–1444. [[CrossRef](#)]
37. Jost, K.H.; Ziemer, B.; Seydel, R. Redetermination of the structure of β -dicalcium silicate. *Acta Crystallogr. Sect. B Struct. Crystallogr. Cryst. Chem.* **1977**, *33*, 1696–1700. [[CrossRef](#)]
38. Tasker, P.W. The stability of ionic crystal surfaces. *J. Phys. C Solid State Phys.* **1979**, *12*, 4977–4984. [[CrossRef](#)]
39. Noguera, C. Polar oxide surfaces. *J. Phys. Condens. Matter* **2000**, *12*, R367–R410. [[CrossRef](#)]
40. Tao, Y.; Zhang, W.; Li, N.; Ching, W.-Y.; Wang, F.; Hu, S. Atomic-level insights into the influence of zinc incorporation on clinker hydration reactivity. *Open Ceram.* **2020**, *1*, 100004. [[CrossRef](#)]
41. Hewlett, P.C.; Liska, M. *Lea's Chemistry of Cement and Concrete*; Butterworth-Heinemann: Oxford, UK, 2019.
42. Chan, C.-J.; Kriven, W.M.; Young, J.F. Analytical Electron Microscopic Studies of Doped Dicalcium Silicates. *J. Am. Ceram. Soc.* **1988**, *71*, 713–719. [[CrossRef](#)]

